Observing the Phase Space Trajectory of an Entangled Matter Wave Packet

U. Poschinger,* A. Walther, K. Singer, and F. Schmidt-Kaler

Institut für Quantenphysik, Universität Mainz, Staudingerweg 7, 55128 Mainz, Germany

(Received 30 May 2010; revised manuscript received 28 October 2010; published 20 December 2010)

We observe the phase space trajectory of an entangled wave packet of a trapped ion with high precision. The application of a spin-dependent light force on a superposition of spin states allows for coherent splitting of the matter wave packet such that two distinct components in phase space emerge. We observe such motion with a precision of better than 9% of the wave packet extension in both momentum and position, corresponding to a 0.8 nm position resolution. We accurately study the effect of the initial ion temperature on the quantum entanglement dynamics. Furthermore, we map out the phonon distributions throughout the action of the displacement force. Our investigation shows corrections to simplified models of the system evolution. The precise knowledge of these dynamics may improve quantum gates for ion crystals and lead to entangled matter wave states with large displacements.

DOI: 10.1103/PhysRevLett.105.263602 PACS numbers: 42.50.Dv, 03.65.Ta, 03.67.Bg, 03.67.Mn

Entanglement of matter is a fascinating subject, as it represents the fundamental feature of quantum physics. Its observation in experimental realizations of former Gedanken experiments forces us to abandon any classical imagination of particles or matter waves. Beyond these considerations, entanglement is a resource for important tasks, including information processing and precision measurements. In the last decade, we have witnessed a growth of experiments with well-defined quantum systems, the most prominent among them being atomic two-level systems (qubits) [1]. For trapped ions, quantum gates are based on the transient entanglement between qubit and external (motional) degrees of freedom, which is mapped onto the qubit state, such that the motion is finally disentangled from the qubit. High fidelity gate operations are only possible if no information is left in the motional degrees of freedom. Therefore, a high degree of motional control is required, for which it is of interest to precisely monitor the coupled dynamics of spin and motion. The focus of this Letter is the entanglement of the spin of a trapped ion with its motional state by means of laser driven displacement operations as proposed in Refs. [2] and experimentally realized, e.g., in [3–6]. We present an analysis of the dynamics both in phase space and in Hilbert space, where we sense higher-order terms of the ion-light interaction Hamiltonian. We are able to reveal experimentally that quantum superpositions of coherent states are increasingly difficult to control when the displacement magnitude becomes larger. Our work is of importance for the investigation of the scalability of quantum information processing based on trapped ions. This Letter is organized as follows: First, we describe how to prepare our qubit and how we generate and manipulate entangled states. We then present data which elucidate the role of the initial ion temperature for the dynamics driven by the spin-dependent force. We show three ways to analyze the dynamics of the optically driven ion: First, we use decay and revival of the spin contrast for extraction of displacement magnitudes. The second approach consists of a more detailed measurement of the motional state by mapping out phonon distributions. A third approach maps out the dynamics in phase space by means of a wavepacket homodyning technique, which allows us to follow the ion's trajectory with high precision. While the first scheme is sufficient to set the laser interaction parameters for gate operations, it does not provide conclusive information about error sources, except for the effect of initial thermal excitation, which we accurately match to a theoretical model. This method characterizes the quantum state only partially as only overlap integrals along one direction in phase space are measured, relying on assumptions on the initial state. The second scheme gives partial information about the dynamics in Hilbert space; i.e., diagonal elements of the density matrix characterizing the quantum state in phonon number representation can be extracted. It can be extended to a complete tomography scheme [7]. A third approach based on wave function homodyning works even outside the Lamb-Dicke regime and provides an accurate and simultaneous measurement of position and momentum expectation values. Furthermore, it represents an efficient way for complete quantum state tomography, as it is pointed out in [8].

We use a microstructured Paul trap [9], which provides harmonic confinement with frequencies of $\omega/(2\pi) = \{1.35, 2.4, 3\}$ MHz for a single $^{40}Ca^{+}$ ion, where the lowest frequency ω_{ax} pertains to the axial vibrational mode. We apply Doppler cooling on the $S_{1/2}$ to $P_{1/2}$ transition near 397 nm. A magnetic field of about $B = 0.4$ mT splits both Zeeman qubit-levels of the ground state $S_{1/2}$, labeled $\{|\uparrow\rangle, |\downarrow\rangle\}$, by 18 MHz. We initialize the ion by ground state cooling [10], followed by optical pumping to $|\uparrow\rangle$. For qubit manipulations drive stimulated Raman transitions: the ion is irradiated by two laser beams near 397 nm at detunings in the range between $\Delta/(2\pi) = 40$ GHz and 100 GHz from the dipole transition. To perform different operations

we utilize three different beam geometries: (i) Two copropagating beams, $R1$ and CC, orthogonal to the direction of B with a relative detuning corresponding to the Zeeman splitting, drive single qubit rotations without coupling to any motional degrees of freedom. Both beams have a linear polarization, aligned according to $R1 \parallel B$ and $\mathrm{CC} \perp B$. (ii) Two beams, $R1$ and $R2$, with $R2$ propagating in parallel to the magnetic field and $R1$ propagating orthogonally to $R2$, both beams are aligned at 45° with respect to the trap axis. $R1$ and $R2$ establish a beat pattern with a difference vector δk along the trap axis enabling momentum transfer. Qubit rotations may be driven with a coupling to the ion's axial mode, characterized by a Lamb-Dicke factor $\eta = \Delta k x_0 \approx 0.25$, where x_0 is the ground state wave packet extension. This geometry is used for to drive Rabi oscillations on motional sidebands. (iii) A third pair of beams is comprised of $R2$ and CC, where only circular polarization components are present such that no coupling of the qubit levels occurs, but axial motion can be excited via an ac-Stark light force oscillating close to the vibrational frequency. Phase and magnitude of this drive depend on the qubit state [4,5]. By adjusting the $R2$ polarization, the force can be set to displace only one spin component (purely circular), the two spin components in the same direction (linear in-plane with CC propagation direction) or the two spin components in different directions (linear orthogonal to CC). After performing manipulations on the spin and the motional state, the spin is read out by transferring the population from $|\uparrow\rangle$ to the metastable $D_{5/2}$ state via a rapid adiabatic passage pulse [10]. When illuminated with resonant light near 397 nm, the ion is measured to be in $|\downarrow\rangle$ if we detect fluorescence, and in $D_{5/2}$ (corresponding to $|\uparrow\rangle$) otherwise. We repeat the sequence 200 times to determine the spin occupation probabilities $P_\uparrow$ and $P_\downarrow$. We generate entangled wave packets with the sequence in Fig. 1(a). Laser configuration (i) is employed for the spin-echo pulses and configuration (iii) for the spin-dependent displacement. For balanced circular polarization components of the $R2$ beam, the Schrödinger picture Hamiltonian for the light-matter interaction reads

$$\hat{H}_S = -\hbar \Delta_S \sin(\Delta k \hat{x} - \delta_{R2,\mathrm{CC}} t + \Delta\phi_{R2,\mathrm{CC}}) \hat{\sigma}_z, \qquad (1)$$

where Δ_S is the amplitude of the Stark shift beat pattern of the two beams, $\delta_{R2,\mathrm{CC}} = \omega_{\mathrm{ax}} - \delta$ is the relative detuning, $\Delta\phi_{R2,\mathrm{CC}}$ is the optical phase difference, and $\hat{\sigma}_z$ is the Pauli spin operator. In the Lamb-Dicke limit, where $\langle \Delta k x \rangle \ll 1$ holds throughout the evolution, a displacement pulse acting for time t on a superposition state results in the state [11]

$$|\Psi_f\rangle = \frac{1}{\sqrt{2}}(|\uparrow, \alpha(t)\rangle + i|\downarrow, -\alpha(t)\rangle),$$
$$\alpha(t) = -\frac{\eta \Delta_S}{2\delta} e^{i\delta t/2} \sin\frac{\delta t}{2}. \qquad (2)$$

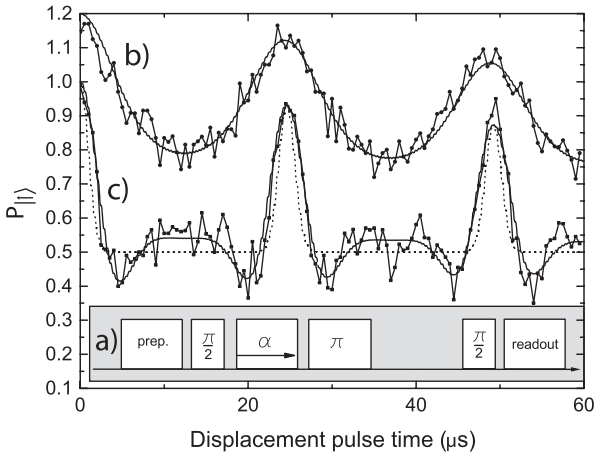

FIG. 1. Time evolution of entanglement and disentanglement for a ground state wave packet: (a) Experimental pulse sequence, see text. The gaps in the spin-echo sequence have a duration of 100 μs. The phase contrast as a function of displacement pulse duration is shown for (b) a ground state ion, and (c) a Doppler cooled ion. The solid lines result from a fit to Eq. (3), as described in the text, and the dashed line indicates the prediction of Eq. (2) in Ref. [4], neglecting the nonclassical dependence of the force magnitude on the motional state. Note that curve (b) is shifted upwards by 0.2 for better visibility.

When the concluding $\pi/2$-pulse acts on this state, the spin will only flip completely into $|\uparrow\rangle$ if no displacement was present, since this can be seen as a which-path information, suppressing the spin interference. The fringe contrast is given by the overlap of the adjacently displaced ground state wave packets: $\mathcal{C}(t) = |\langle -\alpha(t)|\alpha(t)\rangle|^2 = e^{-2|\alpha(t)|^2}$, thus serving as a measure of the displacement magnitude. As the motion is driven slightly off-resonant with $\delta_{R2,\mathrm{CC}}$, the spin is periodically entangled and disentangled with the motion, and we observe the coherence decay and revive. The data plotted in Fig. 1(a) show the dynamics of $P_\uparrow(t)$ at the end of the sequence, indicating that the wave packets of both spin components are driven back into the origin after about 24 μs, as expected from $\delta = 2\pi \times 42$ kHz. For applications of the displacement operation, it is of interest to investigate the effect of an initial thermal excitation of the motional state. Figure 1(b) shows the contrast signal for a Doppler cooled ion with an average phonon number $\bar{n} \approx 20$. For this and the following measurements in this Letter, an empirical exponential decay $e^{-\gamma t}$ for laser interaction times t is included to account for laser induced decoherence [12]. The expression for the contrast is obtained by thermal averaging with displacements $\alpha_n(t)$ that depend on n:

$$\mathcal{C}(t) = e^{-\gamma t} \sum_n p_n^{(i)} |\langle n, -\alpha_n(t)|n, \alpha_n(t)\rangle|^2. \qquad (3)$$

Here, $p_n^{(i)}$ is the initial thermal phonon distribution. The displacements $\alpha_n(t)$ are determined by a quantum dynamical simulation: The time-dependent 1D Schrödinger

equation for the harmonically bound ion subject to the time-dependent control laser field is solved by means of a Chebshev propagator technique in conjunction with a Fourier grid [13]. The displacement is obtained from the position and momentum expectation values. The resulting thermal average of Eq. (3) is plotted as the solid line in Fig. 1(c), and is in good agreement with the experimental data. Previously used models, such as the one in Ref. [4], do not include the n dependence of the displacement force and do not correctly reproduce the data. The dependence of the force magnitude on n is of importance for multi-ion entangling gate operations in the thermal regime [14], where the thermal dispersion of trajectories can be among the main sources of infidelity. The light-force mediated entanglement operation can be investigated not only in terms of spin coherences, but also by directly monitoring the motional degree of freedom. We drive the displacement dynamics and analyze the resulting motional state with the sequence in the inset of Fig. 2 by using the Raman beams in configuration type (ii), where resonant Rabi oscillations on the blue motional sideband (bsb) contain information on the motional state, i.e., the occupation probabilities p_n of

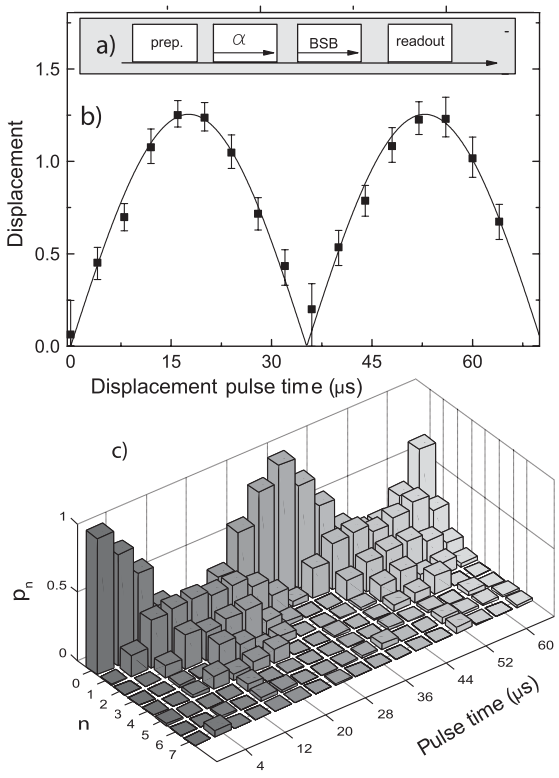

FIG. 2. Phonon distribution dynamics: (a) The experimental measurement sequence, see text. (b) Measured displacement parameter versus displacement pulse time obtained from the measured phonon distributions, the solid line is a fit to Eq. (2). (c) Reconstructed phonon distributions $p(n)$ from the blue sideband Rabi oscillations. The typical confidence intervals are up to ± 0.1 for the displaced states and about ± 0.05 for the states with small or no displacement.

the number states $|n\rangle$ [15]. The resonant bsb excitation for a pulse time t_p results in a signal

$$P_{|\downarrow\rangle}(t_p) = \sum_n \frac{p_n}{2}(ae^{-\gamma t}\cos(\Omega_{n,n+1}t_p) + 1). \quad (4)$$

To obtain the p_n along with the parameters Ω_0, a and the decoherence rate γ, we employ a maximum-likelihood reconstruction by means of a genetic algorithm [16]. Blue sideband Rabi frequencies of $\Omega_0 = 2\pi \times 28(2)$ kHz and decay rates between $\gamma = 5 \times 10^3$ s^{-1} and $\gamma = 11 \times 10^3$ s^{-1} are attained, where γ increases with the motional excitation as the faster bsb Rabi oscillations are more sensitive to intensity fluctuations [15]. Simulations confirm that the decoherence rates and their behavior on the motional state is consistent with a shot-to-shot fluctuation of the Rabi frequency of about 4% around its mean value. The residual Stark shift of less than 10 kHz is assumed not to contribute significantly to the dephasing. The resulting phonon distributions for the various displacement pulse times can be fit to distributions pertaining to a coherent state, $p_n(\alpha) = e^{-|\alpha|^2}|\alpha|^{2n}/n!$. The resulting values $\alpha(t)$ are shown in Fig. 2(a), where one can clearly observe the periodical excursion of the wave packet. The measured phonon distributions in Fig. 2(b) indicate even more strikingly how the light-force driven motion returns the ion back to the vibrational ground state near times of 30 μs. For mapping of the wave packet dynamics, we employ a wave packet homodyning technique [5]; see Fig. 3(a). The spin superposition state formed by the $\pi/2$ pulse is affected by the light force from the type (iii) laser interaction such that only the $|\downarrow\rangle$ component is displaced by $\alpha e^{-i\delta t/2+\phi_1}$ while $|\uparrow\rangle$ remains unaffected. The π pulse flips both spin states, and now a second type (iii) displacement pulse acts on the wave packet component which was left before at $\alpha = 0$. While the amplitudes are equal, the phase ϕ_2 of the second drive pulse is varied, such that both spin components only partially overlap, depending on the difference $\Delta\phi = \phi_2 - \phi_1$. When the sequence is concluded by the last $\pi/2$ pulse, the width and the phase of the interference pattern, Fig. 3(b), allow for determining the magnitude and phase of α. The upper spin state occupation probability finally reads [5]

$$P_{\uparrow}(t) = \tfrac{1}{2}(1 - e^{-|\alpha|^2[1-\cos\phi(t)]-\gamma t}\cos[|\alpha|^2\sin\phi(t)]). \quad (5)$$

Here, $\phi(t) = \Delta\phi + \delta t + \delta t_w$ is the oscillator phase picked up during the driving and idle times in the sequence, denoted by t and t_w, respectively. Sets of $P_{\uparrow}$ were recorded for displacement pulse durations ranging from 0 μs to 76 μs in steps of 4 μs for varying beat phases $\Delta\phi$, and the data are fit to Eq. (5). The extent up to which the dynamics can be followed is limited by the decoherence rate of $\gamma = 13(1) \times 10^3$ s^{-1}. The resulting displacements $\alpha(t)$ are plotted in Fig. 3(c). We can clearly identify deviations from the idealized dynamics, as the wave packet excursion approaches the wavelength of the driving light

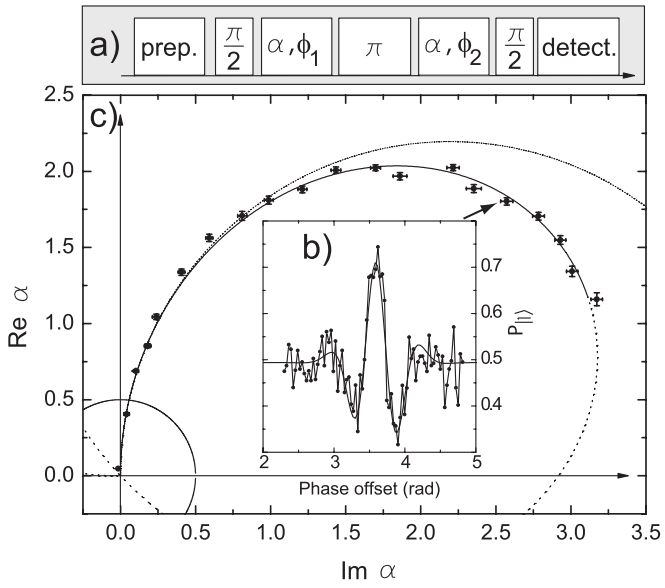

FIG. 3. (a) Trajectory measurement pulse scheme; see text. (b) Homodyne wave function beat signal, for a displacement pulse of length $t = 60\ \mu$s along with a fit to Eq. (5). (c) The resulting phase space coordinates $|\alpha|e^{i\phi}$ inferred from fitting the measured signals $P_\uparrow(\phi)$ to Eq. (5), along with the theoretical trajectory Eq. (2). The outer dashed circle indicates the trajectory that would be observed in the case of a spatially homogeneous force. The circle around the origin indicates the $e^{-1/2}$ radius of the Wigner function, more than 10 times larger than our maximum measurement errors in α.

wave and the Lamb-Dicke approximation fails. The phase $\phi(t)$ is given by the center of the envelope in the beat signal. From the time dependence of $\phi_0(t)$, we obtain the detuning δ with high precision, it is found to be $2\pi \times 5.237(27)$ kHz. We thus determine the vibrational frequency with a relative accuracy on the order of 10^{-5}. Our homodyne measurement scheme can be seen as a continuous variable analog of Ramsey spectroscopy. In order to attain a comparable performance with conventional Ramsey pulses, one would require long delay times of tenths of ms. From the data plotted in Fig. 3(c), one can recognize the deviation from the circular trajectory predicted by Eq. (2). Because of the shallowing of the sine potential Eq. (1) for large excursions $\Delta kx \propto 1$, the maximum excursion of the wave packet is reduced with respect to Eq. (2) for longer driving pulses, which can be accounted for by empirically introducing a reduced effective return time $t_{\mathrm{ret}}^{\mathrm{eff}}$ [6], corresponding to an effective detuning $\delta_{\mathrm{eff}} > \delta$ in the sine function argument in Eq. (2). A fit to the modified Eq. (2) reveals an effective detuning of $\delta_{\mathrm{eff}} = 2\pi \times 6.63(10)$ kHz. The trajectory can be reconstructed only up to an unknown angle of rotation around the origin, given by the relative optical phase between the $R2$ and CC beams at the ion location, which is varying from shot to shot. The measurement accuracies along both axes are much smaller than the dimension of the ground state wave packet size $\sqrt{\hbar/2m\omega_{\mathrm{ax}}}$, which is about 9.5 nm. This does of course not violate the uncertainty principle, as the measurement is statistical and its accuracy relies on the shot-to-shot reproducibility. Quantum simulation, e.g., of random walks [17] may benefit from our method for a precise observation of the wave packet dynamics.

In conclusion, we were able to follow the trajectory of the entangled wave packets. We could measure the contribution of higher-order terms of the interaction to the wave packet dynamics. In the future, we envisage to control the displacement magnitude with a temporally tailored light force. Furthermore, in our experiments we could show how the initial affects the light-force drive and describe this by the correct model. This could be of importance for devising gate schemes more robust than the current ones.

We acknowledge financial support by the European commission within EMALI and the STREP-MICROTRAP, the IPs SCALA and AQUTE.

*poschin@uni-mainz.de

[1] J. I. Cirac and P. Zoller, Phys. Rev. Lett. **74**, 4091 (1995); R. Blatt and D. J. Wineland, Nature (London) **453**, 1008 (2008); J. M. Raimond, M. Brune, and S. Haroche, Rev. Mod. Phys. **73**, 565 (2001).
[2] K. Mølmer and A. Sørensen, Phys. Rev. Lett. **82**, 1835 (1999); G. J. Milburn *et al.*, Fortschr. Phys. **48**, 801 (2000); E. Solano, R. L. de Matos Filho, and N. Zagury, Phys. Rev. A **59**, R2539 (1999).
[3] D. Leibfried *et al.*, Nature (London) **438**, 639 (2005); C. F. Roos, New J. Phys. **10**, 013002 (2008).
[4] P. C. Haljan *et al.*, Phys. Rev. Lett. **94**, 153602 (2005).
[5] C. Monroe *et al.*, Science **272**, 1131 (1996).
[6] M. J. McDonnell *et al.*, Phys. Rev. Lett. **98**, 063603 (2007).
[7] D. Leibfried *et al.*, Phys. Rev. Lett. **77**, 4281 (1996).
[8] P. J. Bardroff, M. T. Fontenelle, and S. Stenholm, Phys. Rev. A **59**, R950 (1999).
[9] S. Schulz *et al.*, Fortschr. Phys. **54**, 648 (2006).
[10] U. G. Poschinger *et al.*, J. Phys. B **42**, 154013 (2009).
[11] D. Leibfried *et al.*, Nature (London) **422**, 412 (2003).
[12] R. Ozeri *et al.*, Phys. Rev. A **75**, 042329 (2007); C. Di Fidio and W. Vogel, Phys. Rev. A **62**, 031802 (2000); Q. A. Turchette *et al.*, Phys. Rev. A **62**, 053807 (2000).
[13] K. Singer *et al.*, Rev. Mod. Phys. **82** 2609 (2010).
[14] G. Kirchmair *et al.*, New J. Phys. **11**, 023002 (2009); G. Kirchmair *et al.*, Nature (London) **460**, 494 (2009).
[15] D. M. Meekhof *et al.*, Phys. Rev. Lett. **76**, 1796 (1996); M. Brune *et al.*, Phys. Rev. Lett. **76**, 1800 (1996).
[16] http://lancet.mit.edu/ga.
[17] H. Schmitz *et al.*, Phys. Rev. Lett. **103**, 090504 (2009).